A multimodal MRI study of functional and structural changes in concomitant exotropia

RUI HAO[1*], YANG WANG[2*], KAILEI WANG[1], ANG WEI[3] and WEI ZHANG[1]

[1]Department of Pediatric Ophthalmology and Strabismus, Tianjin Eye Hospital, Clinical College of Ophthalmology of Tianjin Medical University, Nankai University Affiliated Eye Hospital, Tianjin Key Lab of Ophthalmology and Visual Science, Tianjin Eye Institute, Tianjin 300020; [2]Department of Radiology, Tianjin Medical University General Hospital, Tianjin Key Laboratory of Functional Imaging, Tianjin 300052; [3]Department of Ophthalmology, Tianjin Hospital of Integrated Traditional Chinese and Western Medicine, Nankai Hospital, Tianjin 300102, P.R. China

Received March 19, 2023; Accepted June 19, 2023

DOI: 10.3892/etm.2023.12141

Abstract. The present prospective study aimed to investigate the structural and functional changes in patients with concomitant exotropia using multimodal MRI. A total of 11 adult patients with concomitant exotropia (5 males and 6 females) and 11 healthy adult individuals (5 males and 6 females) were recruited and examined using multimodal MRI techniques. Near and distance exotropia deviation angles were measured. The structrual changes were evaluated using the gray matter volume. Functional reorganization was assessed using the amplitude of low-frequency fluctuation, regional homogeneity and resting-state functional connectivity (FC) on MRI. No significant differences could be found in terms of sex, age or body mass index between the two groups. However, the near and distance exotropia angles were significantly higer in the concomitant exotropia group compared with those in the normal control group (P<0.001). Compared with those in normal individuals, the bilateral thalamus, right middle temporal gyrus (MTG) and right cuneus had significantly reduced gray matter volumes in the concomitant exotropia group (false discovery rate corrected, P<0.05). Reduced FC was found between the bilateral thalamus and the bilateral precuneus, between the right MTG and the right medial superior frontal gyrus in addition to the right precuneus, and between the right cuneus and the right primary sensorimotor cortex (P<0.05, Gaussian random-field corrected) in the concomitant exotropia group compared with that in the normal individuals. In conclusion, the present study indicated that structural and functional reorganization occurs in specific brain regions of patients with concomitant exotropia. These reorganized areas appeared to mainly involve the subcortical structures and related cortices that process visual information.

Correspondence to: Dr Wei Zhang, Department of Pediatric Ophthalmology and Strabismus, Tianjin Eye Hospital, Clinical College of Ophthalmology of Tianjin Medical University, Nankai University Affiliated Eye Hospital, Tianjin Key Lab of Ophthalmology and Visual Science, Tianjin Eye Institute, 4 Gansu Road, Heping, Tianjin 300020, P.R. China
E-mail: zhangwei_eye@163.com

*Contributed equally

Key words: concomitant exotropia, magnetic resonance imaging, gray matter volume, function connectivity

Introduction

Strabismus is a common condition of binocular misalignment, with a prevalence rate ranging from 3-5%, which differs between ethnic groups (1-4). In East-Asian populations, concomitant exotropia is the most prevalent type of strabismus (5,6), which presents as a constant angle of deviation. This condition can lead to visual acuity problems, such as amblyopia and suppression, and further result in deficits in binocular visual function and impact stereopsis.

The pathogenesis of strabismus is mainly associated with the dysplasia of extraocular muscles and surrounding structures, particularly in incomitant strabismus (7,8). However, the association of concomitant strabismus with changes in the central nervous system remains inconclusive. Ocular movement is related to the activity of neurons in specific brain regions, such as the frontal eye field, which is associated with conjugate ocular movement (9,10). It is therefore important to explore the origin of neurons in brain regions.

To evaluate the morphological changes in the entire brain objectively and assess the differences in brain structures, MRI technology may be used. Voxel-based morphometry (VBM) is a technique that allows for the objective evaluation of changes in brain structures (11). The present study utilized the VBM method to analyze the changes in functional brain areas in patients with concomitant exotropia and further expand the knowledge on the pathogenesis of exotropia in the central nervous system.

Subjects and methods

Patients. For the present prospective study, a total of 11 adult patients with concomitant exotropia (5 males and 6 females) who visited the Department of Pediatric Ophthalmology and Strabismus at Tianjin Eye Hospital (Tianjin, China) from October 2021 to March 2022 were recruited. In addition, 11 healthy adult individuals (5 males and 6 females), who were age- and sex-matched, were recruited into the normal control group. All participants underwent complete eye examinations and their corrected visual acuities were 20/20. The dominant eyes were the left eyes and any subjects with organic eye lesions, anisometropia, ocular trauma, surgeries, mental or psychological diseases, systemic diseases and neurological disorders were excluded. All participants were right-handed and ethnic Han individuals, whereas their body height and weight were recorded. The near and distant strabismus angle of patients with concomitant exotropia was also measured. Written informed consent was obtained from all selected subjects and the study was approved by the ethics review committee of Tianjin Eye Hospital (approval no. 2021046; Tianjin, China), according to the Declaration of Helsinki.

MRI data processing

MRI technology parameters. A 3.0 Tesla MRI (Prisma; Siemens Healthineers) was used to acquire the structural and functional images from the subjects. Foam cushions were used to cover the heads of all subjects to minimize movement during imaging. The 3D-magnetization-prepared rapid gradient echo (MPRAGE) sequence was utilized to reconstruct T1-weighted structural images with high resolution. The 3D-MPRAGE sequence parameters were as follows: Repetition time (TR)/echo time (TE), 2,000/2.26 msec; flip angle (FA), 8˚; field of view (FOV), 256x256 mm^2; slice thickness, 1 mm; with 192 slices. Echo-planar imaging (EPI) was used for the resting-state MRI scan. The EPI scan parameters were as follows: TR/TE, 750/30 msec; FA, 54˚; FOV, 222x222 mm^2; slice thickness, 3 mm; interval, 0; and 640 time-points were acquired each time.

Structural MRI data processing. The high-resolution T1-weighted structural images were preprocessed using the statistical parametric mapping software package (SPM12; https://www.fil.ion.ucl.ac.uk/spm/software/spm12) on the MATLAB R2016b platform (The MathWorks, Inc.) and the voxel-based morphometry tool (CAT12; Salford Systems; Computational Anatomy Toolbox; http://www.neuro.uni-jena.de). First, the original images were registered to the standard space of the Montreal Neurological Institute (MNI; https://www.mcgill.ca/bic/software/tools-data-analysis/anatomical-mri/atlases). Next, the standard images were segmented into gray matter, white matter and cerebrospinal fluid (CSF) using tissue segmentation in SPM12. Finally, the gray matter volume (GMV) images were spatially smoothed by a 6-mm Gaussian kernel with full width at half maximum (FWHM). The smoothed images were then used for statistical analysis.

Functional MRI (fMRI) data processing. The resting-state fMRI data were preprocessed using the statistical parametric mapping software package (SPM12) on the MATLAB R2016b platform and the DPARSF_V5.3 software (http://rfmri.org/DPARSF). The 640 volumes were acquired for functional scanning, where the first 10 time-points were excluded in order to remove the instable data caused by the signal equilibrium and participants' adaption to scanning noise. Slice-timing correction was not applied due to the significantly shortened TR. To remove head movement, head motion correction was performed. The functional images were coregistered with the structural images and spatially normalized using the MNI template. Resampling of each voxel was performed to 3x3x3 mm^3. The spatial smoothing process was then performed using a Gaussian kernel of 6 mm FWHM. The liner drift, band filter, Friston-24 parameters, the mean global signal, the white matter signal and CSF signal were then extracted as covariates and regressed out to minimize non-neural signals.

The amplitude of low-frequency fluctuation (ALFF), regional homogeneity (Reho) and functional connectivity (FC) analyses were perfomed using the DPARSF_V5.3 software. In the ALFF analysis, the time series was converted to the frequency domain using fast Fourier transform. The square root of the power spectrum was also calculated and averaged over 0.01-0.08 Hz. A standardization procedure was applied by dividing the individual ALFF map by its own mean ALFF. The Reho analysis was conducted by calculating the Kendall consistency coefficient of neighboring vertices' blood-oxygen-level dependent time series before the spatial smoothing procedure. For standardization purposes, each individual Reho map was divided by its own mean Reho. Subsequently, all Reho maps were smoothed using 6 mm FWHM. For the FC analysis, the spherical region (3 mm radius) with the spatial coordinates of the significant GMV differences between the groups was used as the regions of interest (ROI). FC analysis was conducted by calculating the correlation coefficient between the average time series of ROIs and residual brain voxels. The ALFF, Reho and FC values of each voxel were transformed by Fisher-Z transformation to obtain the Z-score maps of FC for each subject.

Statistical analysis

Statistical analysis of clinical data and MRI data. The clinical data were analyzed using the SPSS 25.0 software (IBM Corp). The quantitative data of each group were examined for normality of distribution (Shapiro-Wilk test) with a threshold of α=0.05 and expressed as the mean ± standard deviation. An unpaired two-samples t-test was used to compare age, body mass index and deviation angle. The χ^2 test was employed for sex analysis between the groups. $P<0.05$ was considered to indicate a statistically significant difference or association.

Statistical analysis of structural MRI data. An unpaired two-samples t-test was conducted in GMV between the concomitant exotropia group and the normal control group, with sex, age and whole brain volume serving as the covariates. The statistical threshold was $P<0.05$ [false discovery rate (FDR) correction].

Statistical analysis of functional MRI data. The regions with significant GMV differences were used as masks and the ALFF and Reho values of the masks were extracted. The general linear model in the SPSS 25.0 software was used to compare the ALFF and Reho values between the two groups, with sex and age as covariates. The statistical significance level was set at $P<0.05$. The t-statistics maps for each group

Table I. Comparison of baseline data and clinical characteristics between the concomitant exotropia group and the normal control group.

Variable	Concomitant exotropia	Normal control	Statistical parameter	P-value
Sex (male/female)	5/6	5/6	χ^2=0	>0.999
Age, years	29.91±6.75	30.36±6.64	t=-0.159	0.875
BMI, kg/m^2	23.28±1.94	23.52±1.50	t=-0.322	0.751
Near exotropia angle (PD, 33 cm)	-33.18±6.81	-4.45±2.16	t=-13.337	<0.001
Distance exotropia angle (PD, 5 m)	-30.45±5.68	-2.91±1.92	t=-15.234	<0.001

Values are expressed as the mean ± standard deviation or n. PD, prism diopter; BMI, body mass index.

were obtained using an unpaired one-sample t-test (significance threshold set at P<0.05, familywise error correction at the voxel level). The explicit masks for two-samples t-tests were defined as the union of the binarized corrected t-maps of the two groups. Subsequently, two-samples t-tests between groups were performed within the explicit masks, with age, sex and head movement parameters as covariates. The significance threshold was set at P<0.001 corrected for Gaussian random-field (GRF) at the cluster level, corresponding to a corrected P<0.05 at the cluster level. The correlation between GMV, ALFF, Reho and FC values, and strabismus angle were analyzed by Pearson's correlation analysis.

Results

Comparison of baseline data and clinical characteristics between groups. Table I shows the comparison of sex, age, BMI and exotropia angle (near and distance) between the concomitant exotropia group and the normal control group (Table I). There were no significant differences in sex, age or BMI between the two groups. However, the near and distant exotropia angles were significantly higer in the concomitant exotropia group compared with those in the normal control group (P<0.001).

Comparison of GMV between groups. The analysis of GMV differences between the concomitant exotropia group and the normal control group indicated that the bilateral thalamus (t=-6.3, FDR corrected, P<0.05), the right MTG (t=-5.25, FDR corrected, P<0.05 and the right cuneus (t=-2.23, FDR corrected, P<0.05) of the concomitant exotropia group had significantly reduced GMV compared with those in the normal control group (Fig. 1; Tables II and III).

Comparison of ALFF and Reho values between the two groups. After conducting ALFF and Reho analyses, there were no significant differences between the concomitant exotropia and normal control groups (P>0.05). Specifically, in the ALFF analysis, the bilateral thalamus (t=0.10, P=0.74), right MTG (t=-0.07, P=0.95) and right cuneus (t=0.02, P=0.99) exhibited no significant differences between the two groups. Similarly, in the Reho analysis, the bilateral thalamus (t=-1.58, P=0.13), right MTG (t=-1.31, P=0.21) and right cuneus (t=-0.75, P=0.46) did not exhibit any significant differences (Table IV).

Resting-state FC results compared within and between groups. The intra-group one-sample t-test revealed similar FC patterns in the concomitant exotropia group and the normal control group. Strong FC was observed between the bilateral thalamus and the bilateral cerebellum, frontal lobe, left parietal lobe, anterior cingulate and posterior cingulate gyrus in both groups, while the normal control group also showed strong connectivity with the temporal lobe and parietal lobe. The right MTG and right cuneus showed strong FC with several brain regions in both groups, including the bilateral cerebellum, frontal lobe, temporal lobe, parietal lobe, primary sensorimotor cortex, anterior cingulate cortex and posterior cingulate cortex (FEW corrected, P<0.05; Fig. 2). However, a two-sample t-test indicated reduced FC between the bilateral thalamus and bilateral precuneus in the concomitant exotropia group compared with that in the normal control group (GRF corrected, P<0.05). The concomitant exotropia group also had decreased FC between the right MTG and the right medial superior frontal gyrus and the right precuneus (GRF-corrected, P<0.05), as well as reduced FC between the right cuneus and the right primary sensorimotor cortex (GRF-corrected, P<0.05) (Figs. 3 and 4; Tables V and VI).

Correlation analysis between clinical variables and GMV, ALFF values, Reho values and abnormal FC in the concomitant exotropia group. Pearson correlation analysis indicated that the atrophy value of GMV in the bilateral thalamus was positively correlated with the deviation angle (PD) in the concomitant exotropia group (r=0.673, P=0.023). However, no statistically significant correlation was found between the PD and other brain regions of GMV atrophy values, ALFF values, Reho values or FC in the concomitant exotropia group (Tables VII and VIII).

Discussion

Although strabismus is typically characterized by the misalignment of both eyes, with or without abnormal extraocular muscle function, it is currently considered to be a developmental anomaly of the central visual pathway, associated with ocular movement (12). In addition, changes in eye position may lead to developmental changes in binocular vision and stereopsis (13). However, the pathogenesis of concomitant exotropia remains to be fully elucidated. It was previously reported that patients

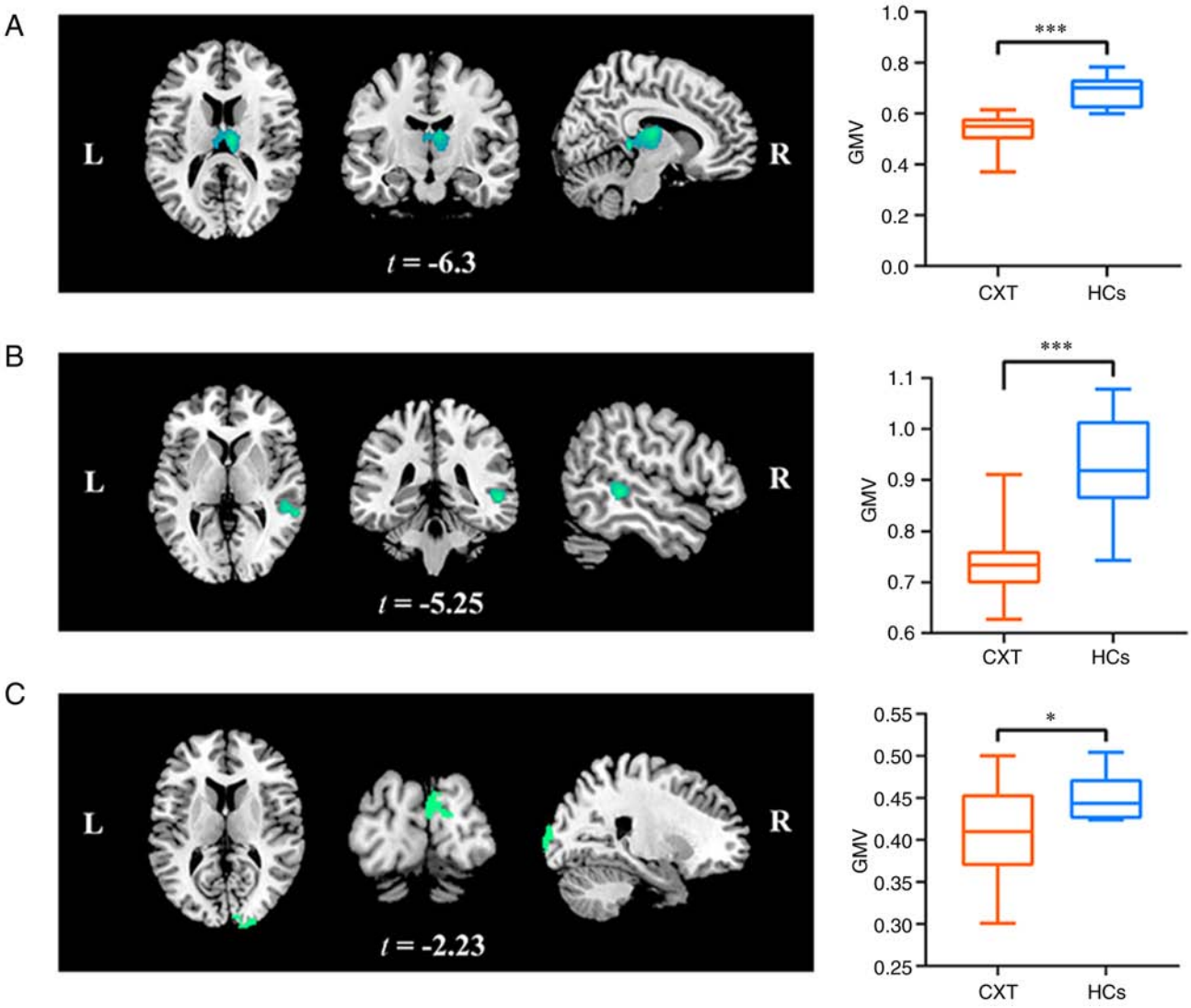

Figure 1. GMV changes between the CXT group and control group. The left column displays brain areas with significantly decreased GMV between the CXT group and control group (P<0.05, false discovery rate corrected). The right column indicates decreased GMV in different brain area clusters between the CXT group (orange) and control group (blue). Decreased GMV in the (A) bilateral thalamus, (B) right MTG and (C) right cuneus. *P<0.05 and ***P<0.001. GMV, gray matter volume; CXT, concomitant exotropia; HCs, healthy controls; L, left; R, right.

with concomitant exotropia exhibit relatively reduced volumes of the medial rectus muscle on MRI, resulting in a relatively weaker function of contraction. This change may be the peripheral mechanism underlying concomitant exotropia (14). However, in addition to this peripheral mechanism, several studies have previously demonstrated that strabismus is associated with abnormal development of the central visual pathway that mediates ocular movement (12,15). A previous study has indicated that early correction of strabismus prevented maldevelopment of ocular movements driven by cerebral motor pathways in a strabismus rhesus monkey model and may be beneficial for brain development in human infants (16).

The dorsal pathway of the visual afferent system exhibits some activation which is not associated with the visuomotor region and it is located more posteriorly, or caudally, to the parietal lobe (17). Previous studies have indicated that MT is related to visual depth perception and may participate in the coding calculation of visual information (18,19). In addition, MT is involved in the processing of parallax signals (20), which is crucial in the coding of three-dimensional information from different sources (21). The present study found a reduction in GMV in the right MTG in patients with concomitant exotropia, suggesting that this change may be associated with a decline of binocular visual function and impairment of stereoscopic function in these patients. A previous study also proposed that the dorsal pathway of the visual afferent system is involved in ocular movement and spatial position information (22), suggesting that abnormal changes in this dorsal pathway may contribute to the development of strabismus.

After the onset of strabismus, alterations in the nervous system are not limited to the visual cortex but can also involve the thalamus (23,24). The thalamus acts as the brain's relay station, with abundant nerve fibers connecting to numerous brain regions (25). A previous study by Chan *et al* (10) revealed that the GMV of the right thalamus was increased in patients with exotropia, which is contrary to the present findings. In the present study, a reduction in the volume of gray matter was observed in the bilateral thalamic region in patients with

Table II. Decreased gray matter volume in the brain regions of the concomitant exotropia group and the normal control group.

Brain region	Location (L/R/B)	MNI coordinates			Voxel size	t-value
		x	y	z		
Thalamus	B	9	-36	3	2,912	-6.30
MTG	R	55.5	-36	-1.5	359	-5.25
Cuneus	R	5	-90	14	820	-2.23

MNI, Montreal Neurological Institute; R, right; L, left; B, bilateral; MTG, middle temporal gyrus.

Table III. Comparison of gray matter volume between the concomitant exotropia group and the normal control group.

Brain region	Location (L/R/B)	Concomitant exotropia group	Normal control group	P-value
Thalamus	B	0.53±0.07	0.69±0.06	<0.001
MTG	R	0.73±0.07	0.93±0.10	<0.001
Cuneus	R	0.40±0.06	0.45±0.03	0.03

R, right; L, left; B, bilateral; MTG, middle temporal gyrus.

Table IV. Comparison of ALFF and Reho values between the concomitant exotropia group and the normal control group.

A, ALFF

Brain region	Location (L/R/B)	Concomitant exotropia	Normal control	P-value
Thalamus	B	0.0034±0.0021	0.0029±0.0042	0.74
MTG	R	0.0163±0.0161	0.0172±0.0349	0.95
Cuneus	R	0.38±0.47	0.38±0.36	0.99

B, Reho

Brain region	Location (L/R/B)	Concomitant exotropia	Normal control	P-value
Thalamus	B	-0.006±0.004	-0.004±0.003	0.13
MTG	R	-0.06±0.02	-0.04±0.03	0.21
Cuneus	R	0.82±0.56	1.02±0.69	0.46

R, right; L, left; B, bilateral; ALFF, amplitude of low-frequency fluctuation; Reho, regional homogeneity; MTG, middle temporal gyrus.

concomitant exotropia. This disparity may be due to differences in the inclusion criteria of patients. However, changes in thalamic function in patients with exotropia have been established and further research is required to unravel the specific changes and underlying mechanisms.

The cuneate lobe, located above the medial surface of the posterior occipital lobe, has been indicated to have a decreased GMV in patients with common strabismus (26). Yan *et al* (27) also previously found changes in the function of the cuneate lobe after analyzing brain FC in resting-state MRI images of 10 patients with concomitant exotropia. The present study on patients with concomitant exotropia also revealed decreased GMV of the cuneate lobe compared with that in the normal control group. The ventral pathway of the human visual afferent system, mainly distributed along the occipitotemporal lobe, is relevant to object recognition (17). In the present study, the cuneate lobe, adjacent to the occipital lobe, atrophied to a certain extent and changed its function. The precuneus, located in front of the cuneate lobe, is an inward part of the parietal lobe located in the cerebral hemisphere, separated from the cuneate lobe by the parietooccipital sulcus. It is related to advanced functions, such as eye movement and visual-spatial processing (28). The FC between the bilateral thalamus and bilateral precuneus was decreased in patients with concomitant

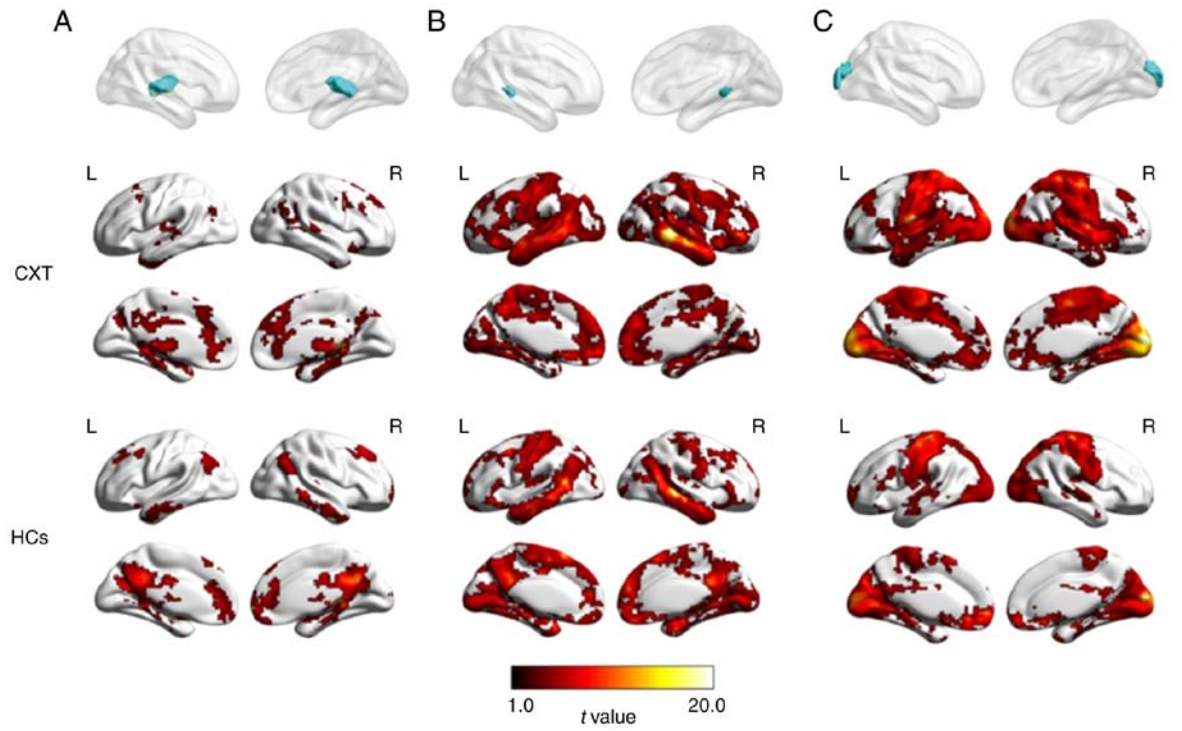

Figure 2. One-sample t-test of FC based on different seeds in the CXT group and control group (P<0.05, family wise error-corrected). (A) FC based on the bilateral thalamus in the CXT group and control group. (B) FC based on the right MTG in the CXT group and control group. (C) FC based on the right cuneus in the CXT group and control group. The color bar represents the t-statistic. FC, functional connectivity; CXT, concomitant exotropia; HCs, healthy controls; MTG, middle temporal gyrus; L, left; R, right.

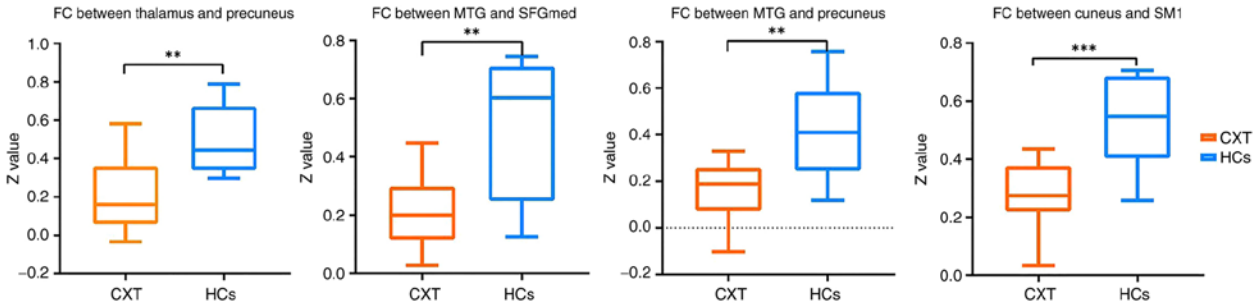

Figure 3. FC changes in different brain area clusters based on different seeds in the CXT group and control group. **P<0.01 and ***P<0.001. FC, functional connectivity; MTG, middle temporal gyrus; CXT, concomitant exotropia; HCs, healthy controls; SFGmed, medial superior frontal gyrus; SM1, primary sensorimotor cortex.

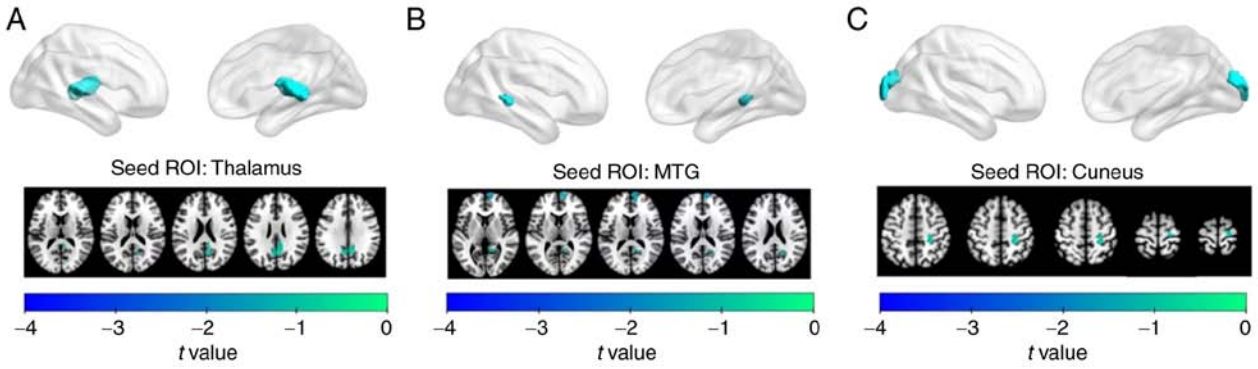

Figure 4. Brain areas with significant FC changes between the concomitant exotropia group and control group (P<0.05, Gaussian random-field corrected). The brain areas showed significant FC changes (A) between the bilateral thalamus and the bilateral precuneus, (B) between the right MTG and the right medial superior frontal gyrus as well as the right precuneus, and (C) between the right cuneus and the right primary sensorimotor cortex. The color bar represents the t-statistic. FC, functional connectivity; MTG, middle temporal gyrus; ROI, region of interest.

Table V. Brain regions with statistically significant differences in functional connectivity values between the concomitant exotropia group and the normal control group.

Brain regions	MNI coordinates			Voxel size	t-value
	x	y	z		
Bilateral thalamus and bilateral precuneus	9	-63	21	203	-3.827
Right MTG and right medial superior frontal gyrus	3	69	9	103	-4.777
Right MTG and right precuneus	21	-57	21	63	-3.968
Right cuneus and right primary sensorimotor cortex	24	-24	51	98	-4.214

MNI, Montreal Neurological Institute.

Table VI. Comparison of functional connectivity values between the concomitant exotropia group and the normal control group.

Brain regions	Concomitant exotropia	Normal control	P-value
Bilateral thalamus and bilateral precuneus	0.21±0.19	0.49±0.17	0.002
Right MTG and right medial superior frontal gyrus	0.21±0.12	0.50±0.24	0.001
Right MTG and right precuneus	0.15±0.13	0.42±0.20	0.001
Right cuneus and right primary sensorimotor cortex	0.28±0.12	0.54±0.16	<0.001

Table VII. Univariate correlation between deviation angle and ALFF as well as Reho values.

A, ALFF

Brain region	R	P-value
Right MTG	-0.390	0.235
Thalamus	0.078	0.819
Right cuneus	0.257	0.445

B, Reho

Brain region	R	P-value
Right MTG	-0.149	0.662
Thalamus	-0.079	0.818
Right cuneus	-0.148	0.665

R, coefficient of correlation; ALFF, amplitude of low-frequency fluctuation; Reho, regional homogeneity; MTG, middle temporal gyrus.

Table VIII. Univariate correlation between deviation angle and GMV as well as FC.

A, GMV

Brain region	R	P-value
Thalamus	0.673	0.023
Right MTG	-0.210	0.534
Right cuneus	-0.024	0.943

B, FC

Brain region	R	P-value
Bilateral thalamus and bilateral precuneus	0.008	0.981
Right cuneus and right primary sensorimotor cortex	-0.019	0.956
Right MTG and right medial superior frontal gyrus	0.289	0.388
Right MTG and right precuneus	0.374	0.257

GMV, gray matter volume; R, coefficient of correlation; FC, functional connectivity; MTG, middle temporal gyrus.

exotropia, as did the FC between the right MTG and the right medial superior frontal gyrus, and that with the right precuneus was reduced. The FC between the right cuneus and the right primary sensorimotor cortex also decreased, suggesting that a series of changes may have occurred in the precuneus region as the GMV decreases. However, further studies are required to understand these changes more fully.

Abnormal visual input, such as amblyopia, and changes in ocular position, may lead to changes in the development of the visual center, resulting in alterations in GMV (29). However, the present study excluded patients with amblyopia and anisometropia in the inclusion criteria, thereby minimizing the effects of abnormal visual experience on the changes in central GMV observed in patients with concomitant

exotropia without visual acuity abnormalities. The present study provides a foundation for further investigation into the changes in relevant central brain areas associated with the occurrence of concomitant exotropia. However, due to the small sample size and different disease courses, it remains uncertain whether other changes and compensatory mechanisms occur in different brain areas, warranting further research and accumulation of data.

In the present study, FC patterns of the brain were investigated in patients with concomitant exotropia and normal controls. The results of the intra-group analysis indicated that the FC patterns were similar in both groups, with the bilateral thalamus showing strong FC with several brain regions. However, the inter-group analysis revealed decreased FC between the bilateral thalamus and bilateral precuneus in patients with concomitant exotropia compared to normal controls. The study also included a correlation analysis between the clinical variables and brain imaging measures in the concomitant exotropia group, revealing a positive correlation between the GMV atrophy value of the bilateral thalamus and deviation angle.

The present study adds to the growing body of literature on the neural mechanisms underlying strabismus. Except for changes in the volume of extraocular muscles (14), the findings suggested that the pathogenesis of concomitant exotropia may involve central mechanisms, as well as abnormal development of the central visual pathway, contributing to the disorder. The results also clarify another idea that the early correction of ocular position deviation may help stabilize eye position and prevent abnormal development of the central visual pathway. However, the limitation of this study is that the sample size is small and the subjects did not undergo surgical treatment. Therefore, the corresponding neural changes pre- and post-operation and at different follow-up times after surgery cannot be compared. Future studies may build on these findings by investigating the causal relationships between FC patterns and clinical variables in patients with concomitant exotropia, as well as exploring potential interventions aimed at improving FC and clinical outcomes in this population.

Acknowledgements

Not applicable.

Funding

The present study was supported by the National Natural Science Foundation of China (grant no. 81800861), the General Project of Tianjin Health Science and Technology Fund (grant no. TJWJ2021MS041), the Natural Science Foundation of Tianjin Grant (grant no. 22JCZDJC00160), the Scientific Research Foundation of Tianjin Education Commission (grant no. 2021KJ222) and the Tianjin Key Medical Discipline (Specialty) Construction Project (grant no. TJYXZDXK-016A).

Availability of data and materials

The datasets used and/or analyzed during the current study are available from the corresponding author on reasonable request.

Authors' contributions

RH and YW wrote the manuscript. YW performed the MRI imaging. RH, YW, KW and AW performed the data analyses. WZ contributed to the conception of the study and revised the manuscript. All authors contributed to the article and have read and approved the final manuscript. RH and YW confirm the authenticity of all the raw data.

Ethics approval and consent to participate

The present study was conducted in accordance with the Declaration of Helsinki and was approved by the Tianjin Eye Hospital Committee on Human Research (approval no. 2021046; Tianjin, China). Written informed consent to participate in this study was obtained from the participants.

Patient consent for publication

Not applicable.

Competing interests

The authors declare that they have no competing interests.

References

1. Caoli A, Sabatini SP, Gibaldi A, Maiello G, Kosovicheva A and Bex P: A dichoptic feedback-based oculomotor training method to manipulate interocular alignment. Sci Rep 10: 15634, 2020.
2. McKean-Cowdin R, Cotter SA, Tarczy-Hornoch K, Wen G, Kim J, Borchert M and Varma R; Multi-Ethnic Pediatric Eye Disease Study Group: Prevalence of amblyopia or strabismus in asian and non-Hispanic white preschool children: Multi-ethnic pediatric eye disease study. Ophthalmology 120: 2117-2124, 2013.
3. Pathai S, Cumberland PM and Rahi JS: Prevalence of and early-life influences on childhood strabismus: Findings from the Millennium Cohort Study. Arch Pediatr Adolesc Med 164: 250-257, 2010.
4. Bruce A and Santorelli G: Prevalence and risk factors of strabismus in a UK Multi-ethnic Birth Cohort. Strabismus 24: 153-160, 2016.
5. Jie Y, Xu Z, He Y, Wang N, Wang J, Lu W, Wu X and Jiao Y: A 4 year retrospective survey of strabismus surgery in Tongren Eye Centre Beijing. Ophthalmic Physiol Opt 30: 310-314, 2010.
6. Li JH, Xie WF, Tian JN, Zhang LJ, Cao MM and Wang L: Changing strabismus surgery distribution at shanxi province eye hospital in Central China. J Pediatr Ophthalmol Strabismus 54: 112-116, 2017.
7. Oh SY, Clark RA, Velez F, Rosenbaum AL and Demer JL: Incomitant strabismus associated with instability of rectus pulleys. Invest Ophthalmol Vis Sci 43: 2169-2178, 2002.
8. Lueder GT, Dunbar JA, Soltau JB, Lee BC and McDermott M: Vertical strabismus resulting from an anomalous extraocular muscle. J AAPOS 2: 126-128, 1998.
9. Ferraina S, Paré M and Wurtz RH: Disparity sensitivity of frontal eye field neurons. J Neurophysiol 83: 625-629, 2000.
10. Chan ST, Tang KW, Lam KC, Chan LK, Mendola JD and Kwong KK: Neuroanatomy of adult strabismus: A voxel-based morphometric analysis of magnetic resonance structural scans. Neuroimage 22: 986-994, 2004.
11. Ashburner J and Friston KJ: Voxel-based morphometry-the methods. Neuroimage 11: 805-821, 2000.
12. Brodsky MC, Fray KJ and Glasier CM: Perinatal cortical and subcortical visual loss: Mechanisms of injury and associated ophthalmologic signs. Ophthalmology 109: 85-94, 2002.
13. Gunton KB, Wasserman BN and DeBenedictis C: Strabismus. Prim Care 42: 393-407, 2015.

14. Hao R, Suh SY, Le A and Demer JL: Rectus extraocular muscle size and pulley location in concomitant and pattern exotropia. Ophthalmology 123: 2004-2012, 2016.
15. Battaglini PP, Battaglia Parodi M, Tiacci I, Ravalico G and Muzur A: Visual representation of space in congenital and acquired strabismus. Behav Brain Res 101: 29-36, 1999.
16. Wong AMF, Foeller P, Bradley D, Burkhalter A and Tychsen L: Early versus delayed repair of infantile strabismus in macaque monkeys: I. Ocular motor effects. J AAPOS 7: 200-209, 2003.
17. Freud E, Plaut DC and Behrmann M: 'What' is happening in the dorsal visual pathway. Trends Cogn Sci 20: 773-784, 2016.
18. Maunsell JH and Van Essen DC: Topographic organization of the middle temporal visual area in the macaque monkey: Representational biases and the relationship to callosal connections and myeloarchitectonic boundaries. J Comp Neurol 266: 535-555, 1987.
19. Albright TD and Desimone R: Local precision of visuotopic organization in the middle temporal area (MT) of the macaque. Exp Brain Res 65: 582-592, 1987.
20. DeAngelis GC and Uka T: Coding of horizontal disparity and velocity by MT neurons in the alert macaque. J Neurophysiol 89: 1094-1111, 2003.
21. Nguyenkim JD and DeAngelis GC: Disparity-based coding of three-dimensional surface orientation by macaque middle temporal neurons. J Neurosci 23: 7117-7128, 2003.
22. Tootell RB, Hadjikhani NK, Mendola JD, Marrett S and Dale AM: From retinotopy to recognition: fMRI in human visual cortex. Trends Cogn Sci 2: 174-183, 1998.
23. Chino YM, Cheng H, Smith EL III, Garraghty PE, Roe AW and Sur M: Early discordant binocular vision disrupts signal transfer in the lateral geniculate nucleus. Proc Natl Acad Sci USA 91: 6938-6942, 1994.
24. Cheng H, Chino YM, Smith EL III, Hamamoto J and Yoshida K: Transfer characteristics of X LGN neurons in cats reared with early discordant binocular vision. J Neurophysiol 74: 2558-2572, 1995.
25. Moustafa AA, McMullan RD, Rostron B, Hewedi DH and Haladjian HH: The thalamus as a relay station and gatekeeper: Relevance to brain disorders. Rev Neurosci 28: 203-218, 2017.
26. Ouyang J, Yang L, Huang X, Zhong YL, Hu PH, Zhang Y, Pei CG and Shao Y: The atrophy of white and gray matter volume in patients with comitant strabismus: Evidence from a voxel-based morphometry study. Mol Med Rep 16: 3276-3282, 2017.
27. Yan X, Wang Y, Xu L, Liu Y, Song S, Ding K, Zhou Y, Jiang T and Lin X: Altered functional connectivity of the primary visual cortex in adult comitant strabismus: A resting-state functional MRI study. Curr Eye Res 44: 316-323, 2019.
28. Min YL, Su T, Shu YQ, Liu WF, Chen LL, Shi WQ, Jiang N, Zhu PW, Yuan Q, Xu XW, *et al*: Altered spontaneous brain activity patterns in strabismus with amblyopia patients using amplitude of low-frequency fluctuation: A resting-state fMRI study. Neuropsychiatr Dis Treat 14: 2351-2359, 2018.
29. Su T, Zhu PW, Li B, Shi WQ, Lin Q, Yuan Q, Jiang N, Pei CG and Shao Y: Gray matter volume alterations in patients with strabismus and amblyopia: Voxel-based morphometry study. Sci Rep 12: 458, 2022.